Spring 5-2018

Photoelectrochemical Investigations on Novel Earth Abundant Solid State Catalysts for Solar Water Oxidation

Nathaniel Branimir Kurtz
University of Southern Mississippi

The University of Southern Mississippi

Photoelectrochemical Investigations on Novel Earth Abundant Solid State Catalysts for Solar Water Oxidation

Nathan Kurtz

A Thesis
Submitted to the Honors College of
The University of Southern Mississippi
In Partial Fulfillment
of the Requirement for the Degree of
Bachelor of Science
in the Department of Chemistry and Biochemistry

May 2018

Approved by:

_____

Wujian Miao, Ph.D., Thesis Adviser
Department of Chemistry and Biochemistry

_____

Vijay Rangachari, Ph.D., Interim Chair
Department of Chemistry and Biochemistry

_____

Ellen Weinauer, Ph.D, Dean
Honors College

Abstract

In light of a looming fossil fuel scarcity, many forms of alternative, clean energy production are being researched in order to provide a more sustainable source of energy production for the future. One area of research is on using novel, abundant catalytic materials in conjunction with semiconducting materials to drive the splitting of water in order to produce hydrogen gas, an energy-rich fuel. Currently, efficiency is limited by the energy bottleneck posed by the oxygen evolution reaction (OER) half of water splitting. In this work, cobalt selenide (CoSe) catalyst paired with the semiconductor iron oxide (Fe_2O_3) has been identified as a particularly promising system. The results in this study show that CoSe is highly active for water oxidation and greatly increases the OER activity as compared to Fe_2O_3 alone. Studies have also been conducted to show the variation in maximum OER activity with changing electrodeposition time of CoSe, and an optimal deposition time has been identified. Using this deposition time, the water-splitting activity of CoSe/Fe_2O_3 was measured under both light and dark conditions. Scanning electron microscope (SEM) images of films have been taken to observe surface morphology and UV-Vis measurements have been taken to confirm the identity of the deposited films.

Keywords: Solar Energy, Solar Water Splitting, Photoelectrochemical, Semiconductor, Catalyst, Sustainability

Dedication

I dedicate this work to my brother, Ben, who has always supported me and celebrated my accomplishments. No one could ask for a better brother.

Acknowledgements

I would like to thank my advisor, Dr. Wujian Miao, for being a continual source of guidance and support. I would also like to thank Arun Siddarth Sridhar, for being a continual source of answers to my never-ending questions. Additionally, I would like to thank the Drapeau Center for Undergraduate Research for partially funding this project through the Eagle SPUR grant.

Table of Contents

List of Tables

List of Illustrations

List of Abbreviations

EDX	Energy-Dispersive X-Ray Spectroscopy
FTO	Fluorine-doped Tin Oxide
HER	Hydrogen Evolution Reaction
OCP	Open Circuit Potential
OER	Oxygen Evolution Reaction
PEC	Photoelectrochemical
SEM	Scanning Electron Microscope
TW	Terawatt

Chapter 1: Introduction

Photoelectrochemical (PEC) water splitting stores solar energy as chemical energy in the form of H_2 gas.[1] The basic components of a PEC cell consist of light, water, and a catalyst.[1] A catalyst is something that reduces the energy required to begin a reaction (activation energy). The energy from light by itself is not enough to drive the reaction, so a catalyst must be added to the system.[2,3] In a PEC cell, there are two reactions occurring, the "oxidation" of water into O_2, and the "reduction" of water into H_2. Oxidation occurs at the photoanode, an electron-deficient material that takes electrons from water, causing O_2 to form. Reduction occurs at the photocathode, an electron-rich material that donates electrons to water, forming H_2. Of the two reactions, oxidation has the highest activation energy. The rate and efficiency of any reaction is limited by its most difficult (energy intensive) step. As such, efficiency can be most readily improved by designing a catalyst that lowers the activation energy of the oxidation half of the cell.[4,5]

To understand the goal of this project, the composition of the photoelectrodes (photoanode/cathode) must be further explained. Each electrode consists of a semiconductor material, usually a transition metal oxide such as titanium oxide or iron oxide, and a catalyst on its surface. Photons (light particles) are absorbed by the semiconductor and converted into electrons and electron-deficient "holes". Electrons are moved to the surface of the photocathode, driving reduction, while the holes are moved to the photoanode, driving oxidation. At the surface of the electrodes, a catalyst reacts with the electrons and holes, respectively, and water to produce H_2 and O_2, respectively.[6] Recent advances have seen promising improvements in oxygen evolution reaction (OER) activity by using catalysts that are based on earth-abundant transition metal chalcogenides and sulfides (M-S, M-Se), such as cobalt selenide, or nickel selenide. These

catalysts are attractive because they are stable, cost-effective, and can be easily deposited on the electrode surface at low temperatures.[7]

Given the promising scope of these materials, there are very limited studies on their application as co-catalysts for photoelectrochemical water splitting and effects of catalyst composition for electrocatalytic and photoelectrocatalytic activity. The main goal of this project is to focus on the photoelectrochemical solar water splitting applications of these co-catalysts tailored at different compositions and deposition conditions, which could lead to the optimization of efficient photoelectrodes for low applied bias water splitting and also possibly result in the fundamental understanding of the role of active catalyst components in the photoelectrode. These proposed studies would be helpful to provoke further investigations in this area and towards the development of tandem solar water splitting cells.

Chapter 2: Literature Review

2.1 Global Energy Crisis and the Need for Solar Energy Storage

One of the most pressing scientific challenges currently being faced is the issue of rising energy needs along with the rapid consumption of fossil fuels. Currently there are sufficient technology and coal reserves to provide enough energy to keep up with centuries' worth of population growth and economic development, but not without environmental catastrophe.[8] The power consumption for the global population of nearly 7 billion people in 2011 was 15 TW (terawatts, 10^{12} W), and these numbers are expected to increase to 30 TW and 9 billion people by 2050.[9] To combat this it is necessary to transition to clean, renewable forms of energy to provide for the increasing global energy needs. Of the sources of renewable energy, solar energy has the potential to deliver 20 TW of the world's energy supply.[8,10] In order for solar cells alone to provide this 20 TW of energy, a total surface area equivalent to France and Germany combined would need to be covered in solar cells, which would require producing 650 m^2 of solar cell panels per second, 24/7 for 365 days per year, for the next 40 years.[9] Besides the daunting logistics needed to accomplish this, as the contribution of solar energy to total energy supply increases, electricity network operators will have increasing difficulty dealing with the intermittent nature of solar energy (day/night cycle, clouds).[9] Thus if the full potential of solar energy is to be exploited, a large-scale method of storing solar energy in the form of fuel will be needed.

2.2 PEC Water Splitting Background

Of the conventional fuels which can be used to store solar energy, hydrogen is the most attractive, having the highest volumetric energy density and being a non-carbon energy source.[11,12] There are several methods[13,14] for producing hydrogen gas from solar energy, such as photocatalytic water splitting, photovoltaic electrolysis, thermochemical conversion,

photobiological hydrogen production, and PEC water splitting. PEC has several major advantages in that hydrogen and oxygen are produced at separate electrodes, avoiding serious safety concerns,[11] and allowing the gasses to be easily separated. It can be carried out at room temperature, and a PEC cell can be constructed entirely out of inorganic materials, lending the system robustness which is difficult to achieve with organic systems.[9]

In a PEC water splitting cell, the energy from light is absorbed by a semiconducting electrode to produce electron hole pairs. The holes drive the oxidation of water to O_2 gas at the anode (Eq. 2.1), and the electrons drive the reduction of water to H_2 gas at the cathode (Eq. 2.2).

$$2H_2O + 4h^+ \rightleftharpoons 4H^+ + O_2 \qquad E^o = 1.23 \text{ V vs NHE} \qquad \text{(Eq. 2.1)}$$

$$4H^+ + 4e^- \rightleftharpoons 2H_2 \qquad E^o = 0 \text{ V vs NHE} \qquad \text{(Eq. 2.2)}$$

Equations 1 and 2 show that the PEC water splitting process has a standard potential of 1.23 V. In actuality, however, an additional "overpotential" is needed to activate the process. Under real conditions the required potential to split water is 1.9-2 V. An ideal PEC system would have the necessary potential provided by the generation and separation of electrons and holes at the interface between the semiconductor and the electrolyte. This has been the pursuit of much research for the past four decades.[15-19]

2.3 Improvements on PEC Performance

Among the advancements made toward improving the efficiency of the PEC cell, the dual-absorber system (Figure 2.1) is notable.[20] This strategy involves using two light absorbing semiconducting materials on each electrode, rather than one. These would then be referred to as the photoanode and photocathode,

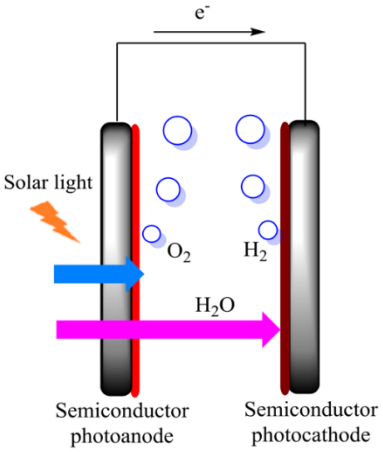

Figure 2.1 Dual Absorber System. Shorter wavelength light (blue) is absorbed by the photoanode (light red) while longer wavelength light (purple) passes through and is absorbed by the photocathode (dark red).

respectively. Using multiple light absorbers allows for an increased range of wavelengths to be absorbed to produce greater numbers of electron hole pairs, producing a greater potential, and thus lowering the overpotential needed.

An essential part in increasing the efficiency of PEC water splitting is the incorporation of catalysts.[21,22] Catalysts are chosen individually for the oxygen evolution reaction (OER) and the hydrogen evolution reaction (HER). Catalysts reduce the kinetic overpotential required to activate water oxidation and reduction, enhance charge separation, prevent electron-hole recombination, and improve the durability of the semiconductor photoelectrodes by protecting them against photocorrosion. The reduction of the required activation energy brings the bias required for water splitting closer to the theoretical value of 1.23 V.

2.4 Improving OER Performance

As the OER is the more energy-intensive half-reaction, much of the current research has been focused on improving the OER catalyst. IrO_2[24,27,28] and RuO_2[23-26] have been the highest performing OER catalysts, however, their cost makes them undesirable, spurring research into earth-abundant non-noble metal-based catalysts. Current research into such alternatives are focused on Ni-, Mn-, and Co-based metal oxides and hydroxides[21] due to their redox properties and stability that is comparable to noble metals. Ni and Co selenides are also emerging as potential new catalysts with good stability and low overpotentials.[29-32] To date, there have been no optimization studies on these new catalysts as to how thickness or composition ratio affects the efficiency of the OER half-reaction in conjunction with a photoanode.

This project will focus on studying CoSe as a catalyst in conjunction with Fe_2O_3 as a photoanode. CoSe is being examined as the catalyst of choice over other cobalt catalysts such as CoP or CoS because of its reported superior performance for OER.[33]

Chapter 3: Methodology

3.1 Electrode Preparation via Electrodeposition

Unless otherwise stated, fluorine-doped tin oxide (FTO) was used as the substrate, and was cleaned by sonication in 3:1 deionized water and ethanolamine solution, followed by deionized water prior to deposition. Electrodeposition is a method of growing thin films in which a conductive substrate is placed in an electrolyte solution containing the salt of the desired film. A potential is applied between the substrate and the counter electrode, causing redox chemistry to take place at the substrate surface, depositing the desired material on the substrate. For some films, a post-deposition thermal annealing was performed at 500 ºC, causing structural rearrangements.[34] The film growth can be optimized by controlling a variety of parameters such as electrolyte composition, pH, potential, and deposition time.[35]

3.2 Performance Measurements

Once the photoanodes were prepared, a variety of methods were employed to characterize the electrodes and measure their performance in terms of photocurrent production, capacitance, charge carrier density, and stability.

3.2.1 PEC Impedance Spectroscopy

Electrochemical impedance spectroscopy is a technique in which an electrochemical system is perturbed by an AC signal of variable frequencies in order to measure the impedance. This provides information on the charge transfer resistance, solution resistance, and double layer capacitance at the electrode-electrolyte interface. This information is usually obtained in the form of Nyquist plots.

3.2.2 Three Electrode *j-V* and Photocurrent Onset Measurements

Three electrode *j-V* and photocurrent onset measurements test a material's ability to produce photocurrent (j_{ph}) at a given potential, and aid in the measurement of photocurrent onset potential (E_{onset}). Figure 3.1 shows a representative three electrode photocurrent measurement for a photoanode.

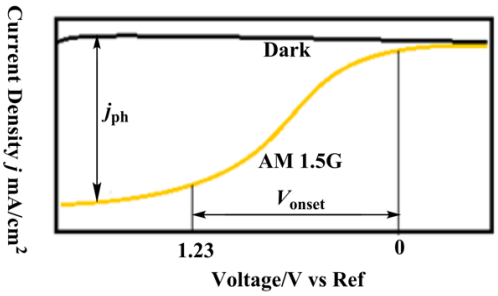

Figure 3.1 A representative linear sweep voltammogram comparing current density under light and dark conditions for a light-sensitive material. As potential is swept from 0 V to 1.23 V, the current density is measured. The difference between the current density under light and dark is the photocurrent. The potential at which current begins to increase is the onset potential.

3.2.3 Stability Measurements

Measurements were made to study how stable the catalyst is after prolonged use by measuring the photocurrent produced at a constant potential and observing how much the photocurrent is reduced over time.

3.3 Characterization

3.3.1 Scanning Electron Microscope (SEM) Imaging

SEM imaging was used to obtain images of the films gown in order to determine their morphology as well as compare their degradation prior to and after stability studies were performed.

3.3.2 Energy-Dispersive X-Ray (EDX) Spectroscopy

EDX spectroscopy will be used to determine the weight percent composition of grown films in order to verify that the films which are grown are in fact of the composition that was intended.

3.3.3 UV-vis Spectroscopy

UV-vis spectroscopy will be used to help determine the band structure of certain materials and films by studying the light absorbed as a result of electron energy transitions.

3.4 Materials

Iron (III) chloride hexahydrate (97%), lithium chloride (99%), cobalt (II) acetate tetrahydrate (reagent grade), sodium tetraborate decahydrate (≥99.5%), and ethanolamine (≥98%) were obtained from Sigma-Aldrich. Sodium fluoride (>99.0%) was obtained from Fluka Chemika. Potassium chloride (A.C.S. reagent) was obtained from Fisher Chemicals. Sodium Selenite (99.75%) was obtained from Alfa Aesar. Deionized water produced using a Millipore Advantage 5 system was used as a solvent for preparing all aqueous solutions.

3.5 Experimental Procedure

3.5.1 Electrode Preparation

Fe_2O_3 photoanodes were prepared by potentiostatic electrodeposition.[34] The working electrode consisted of 1 cm^2 FTO, which was cleaned by sonication in a 3:1 deionized water and ethanolamine solution, followed by deionized water, for 30 minutes each. Ag/AgCl (3.0 M KCl) and Pt foil were used as the reference and counter electrodes, respectively. The deposition was carried out by cycling from -0.47 V to 0.43 V vs Ag/AgCl (3.0 M KCl) for 25 cycles in a bath consisting of 5 mM $FeCl_3$, 0.1 M KCl, 5 mM NaF, and 1 M H_2O_2. The resulting orange-colored films were then rinsed with deionized water, allowed to air dry, and annealed in air at 773 K for 1 h to produce the yellow-orange FTO/Fe_2O_3 electrode for study. The CoSe catalyst was deposited[35] on FTO/Fe_2O_3 by electrodeposition at -0.45 V vs Ag/AgCl (3.0 M KCl) in a bath consisting of 0.065 M $Co(CH_3CO_2)_2$, 0.2 M LiCl, and 0.035 M Na_2SeO_3 at pH 4.7 (adjusted with HCl) to produce the FTO/Fe_2O_3-CoSe photoanode.

Figure 3.2 is the UV-vis spectrum of FTO/Fe_2O_3, showing absorption in the visible region. The absorption edge at 590 nm corresponds to a band gap of 2.10 eV.

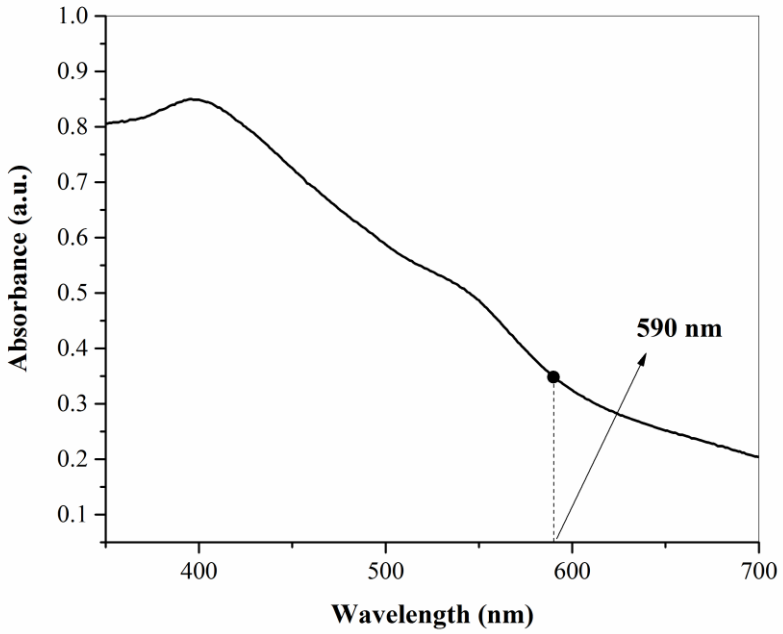

Figure 3.2 UV-vis spectrum of FTO-Fe_2O_3 (Blanked with FTO). The absorption edge at 590 nm corresponds to a 2.10 eV band gap.

3.5.2 Physico-chemical Characterization

Scanning electron microscope (SEM) images and energy-dispersive X-ray data (EDX) of FTO/Fe_2O_3-CoSe were obtained with a Zeiss Sigma VP FEG SEM. An Evolution 300 Thermo-Scientific spectrophotometer was used to obtain the UV-vis spectrum of photoelectrodes, with FTO substrate used as a blank.

3.5.3 Photoelectrochemical Studies

As shown in Figure 3.3, PEC measurements were carried out in a three-electrode setup using a 50-mL quartz beaker as the cell, an Ag/AgCl (3.0 M KCl) as the reference electrode, a Pt wire as the counter electrode, and 1 cm^2 FTO/M (where M = Fe_2O_3 or Fe_2O_3-CoSe) as the working electrode, respectively. A 0.050 M pH 9.0 borate buffer solution was used as the electrolyte for all

experiments with or without the presence of catalyst M of different thicknesses. Electrochemical impedance spectroscopic (EIS) measurements were carried out under open circuit potential (OCP) with a 5.0 mV AC signal superimposed. Mott Schottky plots were obtained at a frequency of 962 Hz. An electrochemical workstation (CH instruments, Model 660 A) was used to conduct electrochemical experiments. Simulated solar light for PEC studies was provided by a 150 W Xe lamp solar simulator (ABET technologies) with an AM 1.5 G filter providing a light intensity of 1000 W/m^2 (1 sun).

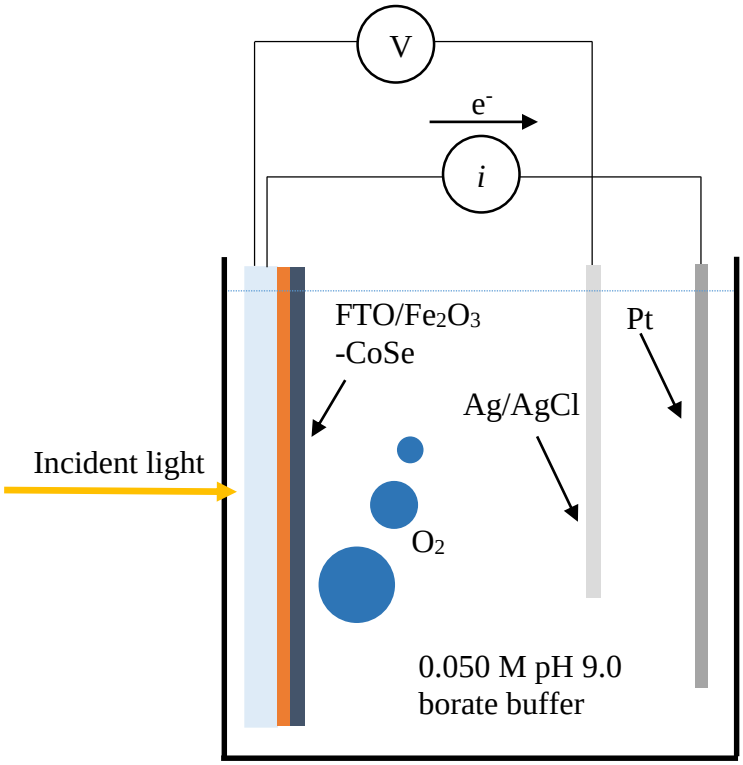

Figure 3.3 Representative cell scheme for photoelectrochemical water splitting using FTO/Fe_2O_3-CoSe. Incident light passes through the transparent conducting working electrode FTO, reaching light-sensitive Fe_2O_3 to generate electrons and holes. Holes move to the catalyst, CoSe, to be used in the OER while electrons move to the Pt counter electrode to be

used in the HER. Current is measured between the working and counter electrode, while potential is measured between the working and Ag/AgCl reference electrode.

Chapter 4: Results and Discussion

4.1 Optimization of FTO/Fe_2O_3-CoSe Films

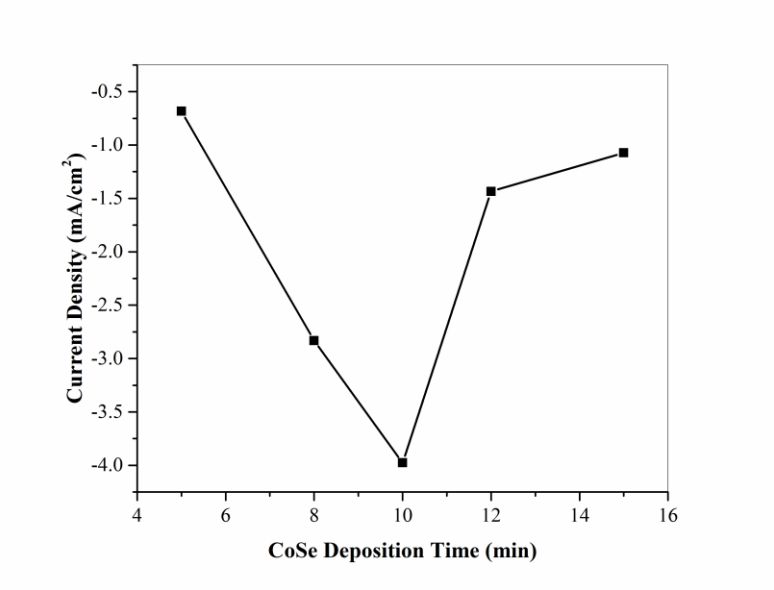

Figure 4.1 CoSe catalyst deposition time vs current density for FTO/Fe_2O_3-CoSe photoanodes at 0.8 V vs Ag/AgCl. The optimal deposition time is shown to be 10 min, producing the most photocurrent.

Figure 4.1 shows the effect of different deposition times of CoSe on current density. Initially, increasing deposition time resulted in increased current density, up to 10 minutes, after which current density decreases with increasing deposition time. This can be attributed to the fact that, at first, as deposition time increases, there is more catalyst assisting in electron/hole separation, resulting in higher OER activity. After 10 minutes, however, the thickness of the film becomes inhibitory due to increased resistance. A thicker film also means that charge carriers are more likely to recombine before being able to participate in water splitting activity. The optimized

deposition time for CoSe on FTO/Fe_2O_3 has been identified as ten minutes, with a maximum photocurrent density of -3.98 mA/cm^2.

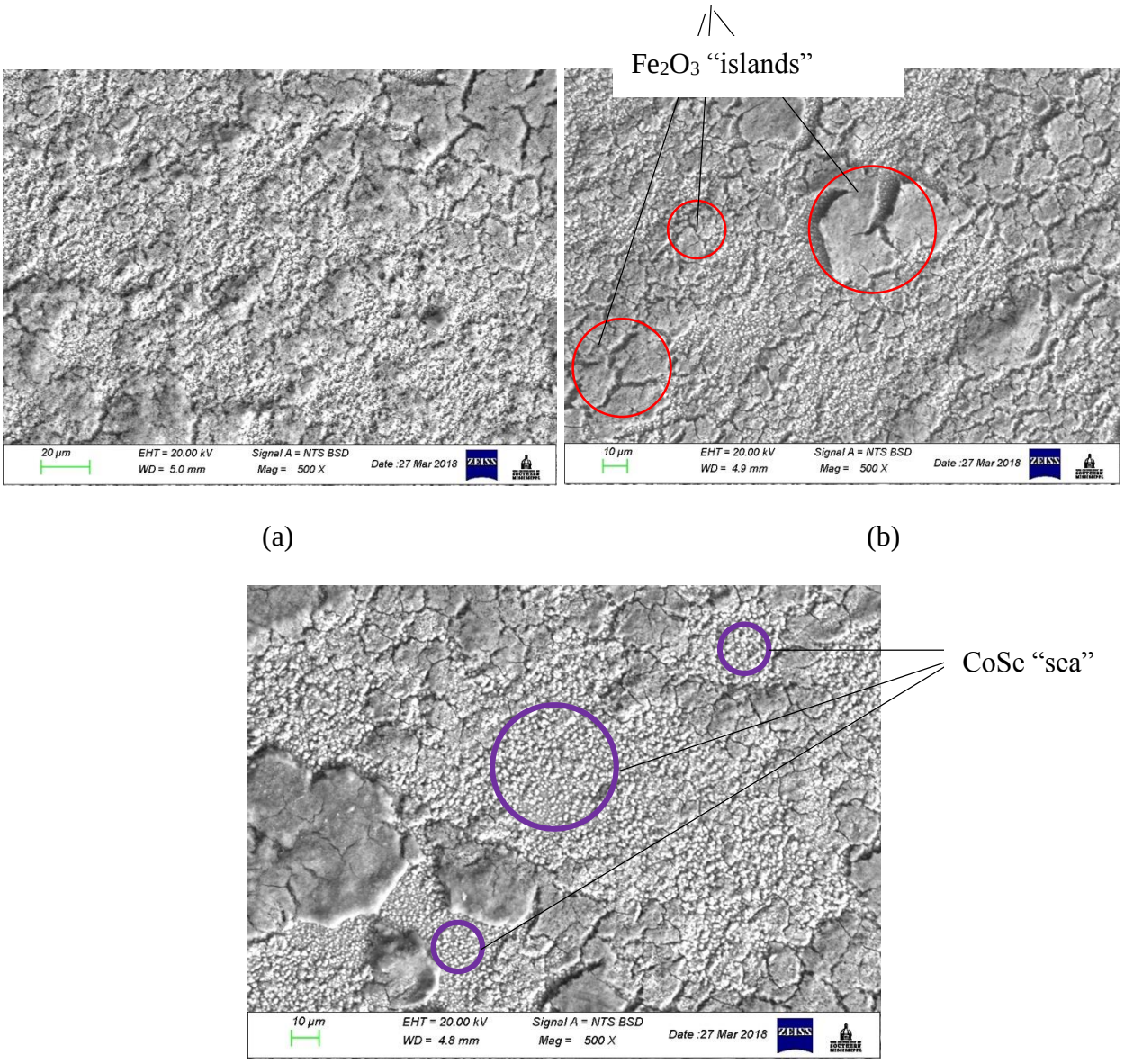

Figure 4.2 500 X magnification SEM images of FTO/Fe_2O_3-CoSe photoanodes at depositions times (a) 5 min, (b) 10 min, and (c) 15 min. This shows "islands" of Fe_2O_3 surrounded by a CoSe "sea," with the amount of CoSe increasing with increasing deposition time.

Figures 4.2a-c and 4.3a-c show SEM images and their corresponding EDX spectra of FTO/Fe_2O_3-CoSe photoanodes at 5-, 10-, and 15-minute deposition times for CoSe, respectively. From the SEM images (Figure 4.2) it can be seen that the Fe_2O_3 is not a single, uniform layer. Rather, the Fe_2O_3 exists as "islands," with CoSe filling the space between the islands. As deposition time is increases, there is a greater amount of CoSe between the islands of Fe_2O_3, similar to a rising sea level. From the EDX map images shown in Figure 4.4, which populate the SEM image with different colors corresponding to different elements, it can be seen that the darker, flat regions correspond to Fe_2O_3, while the lighter, spherical regions correspond to CoSe.

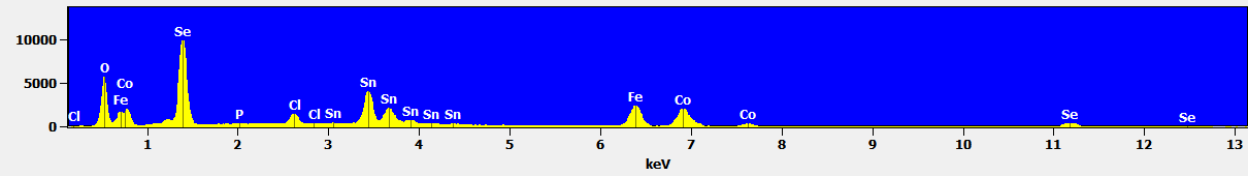

(a)

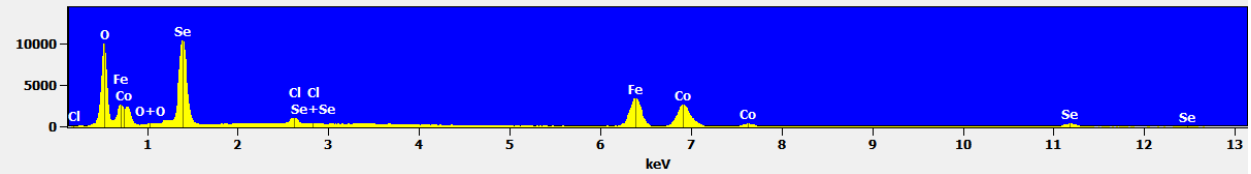

(b)

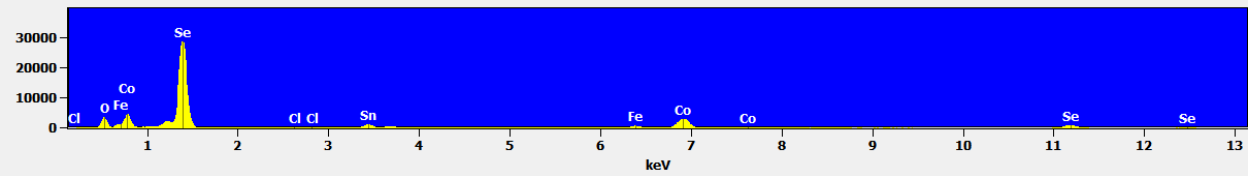

(c)

Figure 4.3 EDX Spectra of FTO/Fe_2O_3-CoSe at deposition times of (a) 5 min, (b) 10 min, and (c) 15 min. The peaks relate the relative number of atoms of particular elements found in the films.

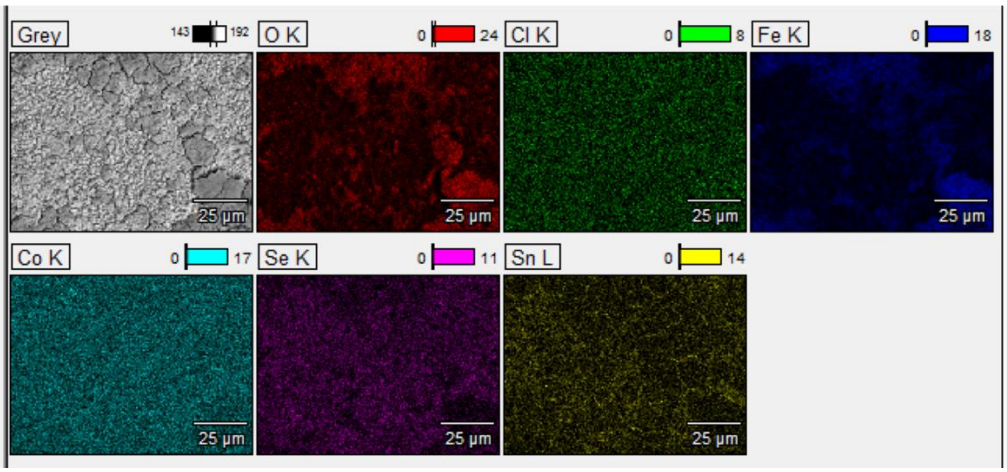

Figure 4.4 EDX color map of 15 min deposition FTO/Fe_2O_3-CoSe. A color is assigned to each element, showing the composition of the films visually. This confirms that the "islands" correspond to Fe_2O_3, since that is where the images are populated by blue (iron) and red (oxygen). Less cyan (cobalt) and purple (selenium) in those regions shows that the CoSe is filling in between the "islands."

Table 4.1 Effects of Deposition Time on CoSe Composition

Parameter	**Time**					
	5 min		10 min		15 min	
Element	Co	Se	Co	Se	Co	Se
Weight %	14.855	19.55	19.99	28.83	24.83	46.18
Mass ratio	0.8	1	0.7	1	0.5	1
Molar ratio	1	1	1	1	1	1.4

Molar ratios of cobalt to selenium were calculated using EDX data, reported in Table 4.1. The EDX data shows that with increasing deposition time, the amount of CoSe by weight percent is increasing. Unlike the 1:1 molar ratio of Co:Se for the 5- and 10-min deposition times, the 15-

minute deposition time shows a molar ratio of 1:1.4, indicating a compositional change at longer deposition times.

4.2 Photocurrent Measurements

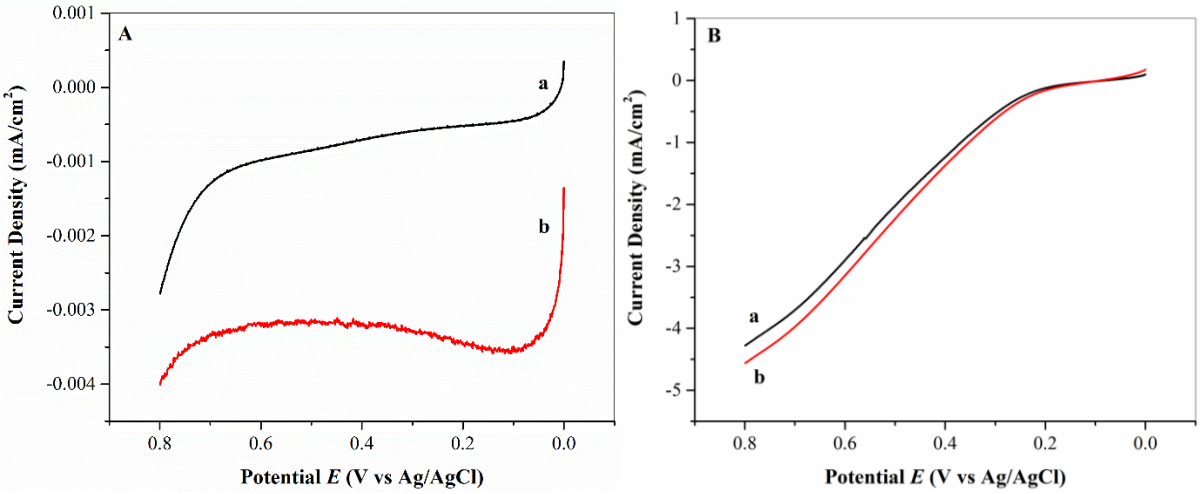

Figure 4.5 (A) Linear sweep voltammograms of FTO/Fe_2O_3 in the absence of catalyst under (a) dark and (b) simulated solar radiation conditions. (B) Linear sweep voltammograms of FTO/Fe_2O_3-CoSe photoanode under (a) dark and (b) simulated solar radiation conditions. Both FTO/Fe_2O_3 and FTO/Fe_2O_3-CoSe show increased photocurrent under light, with FTO/Fe_2O_3-CoSe showing several orders of magnitude higher current density.

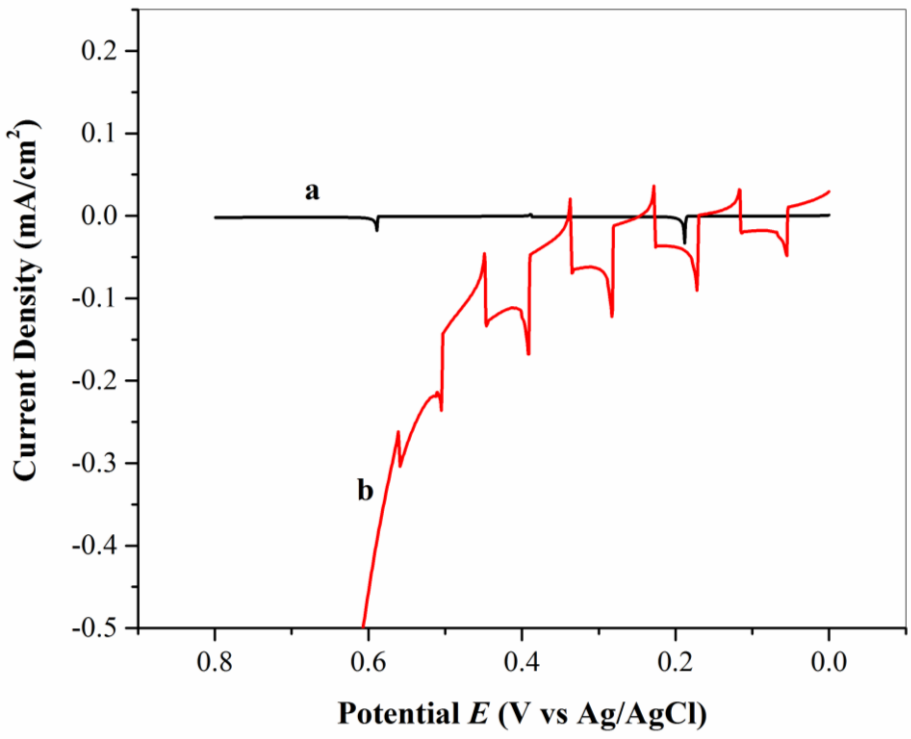

Figure 4.6 Linear sweep voltammograms of FTO/Fe_2O_3 in the (a) absence and (b) presence of catalyst, shuttering light approximately every 3 sec. The large spikes in current for FTO/Fe_2O_3-CoSe show that the addition of CoSe increases charge separation for electrons and holes generated by Fe_2O_3.

The linear sweep voltammograms for FTO/Fe_2O_3 and FTO/Fe_2O_3-CoSe (10 min deposition) photoanodes under dark and irradiated conditions are shown in Figure 4.5. It can be clearly seen that in the presence of CoSe, the OER activity is greatly enhanced. Fe_2O_3 by itself shows a maximum current density of -4.01E-3 mA/cm^2 at 0.8 V vs Ag/AgCl. In the presence of CoSe, the maximum current density achieved was -4.56 mA/cm^2 at 0.8 V. Comparison of the onset potential shows that in the presence of CoSe, a ~0.5 V negative shift in onset potential is observed. Figure 4.6 shows that upon illumination, FTO/Fe_2O_3-CoSe has a much larger photocurrent

response than FTO/Fe_2O_3. This shows that the addition of the CoSe catalyst greatly increases OER activity.

4.3 Electrochemical Impedance Spectroscopy and Mott Schottky Plots

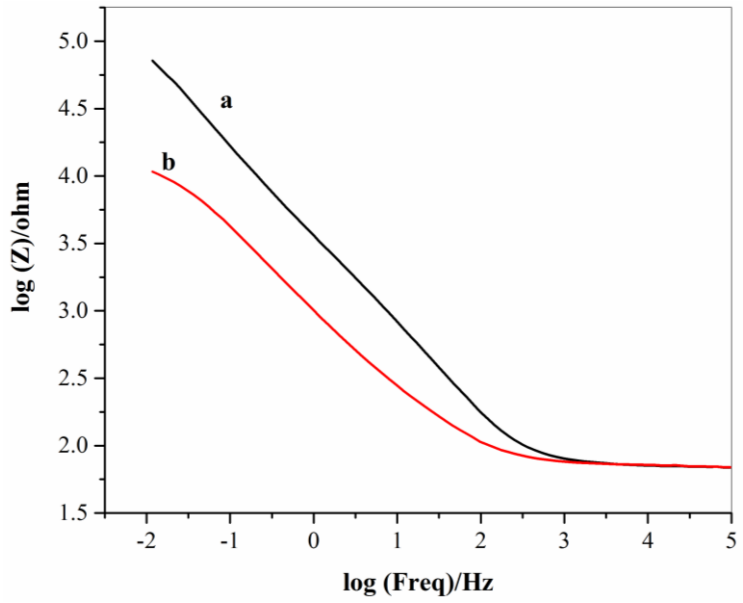

Figure 4.7 Electrochemical impedance spectra of FTO/Fe_2O_3 photoanodes in the (a) absence and (b) presence of CoSe catalyst under simulated solar radiation. The decreased impedance in the presence of catalyst indicates that CoSe improves charge separation.

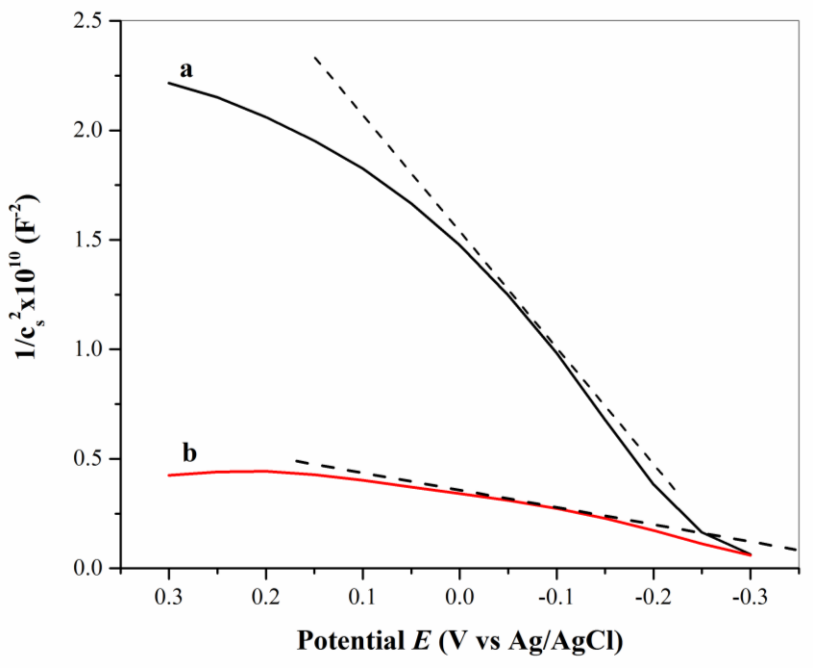

Figure 4.8 Mott Schottky Plots of FTO/Fe_2O_3 photoanodes in the (a) absence and (b) presence of CoSe catalyst under simulated solar radiation. The decreased slope in the presence of catalyst indicates increased capacitance and a greater charger carrier density.

Figure 4.7 shows the EIS measurements comparing FTO/Fe_2O_3 and FTO/Fe_2O_3-CoSe in the form of Bode plots. This can be used to compare the capacitance of the two photoanodes. FTO/Fe_2O_3-CoSe shows a lower maximum impedance, indicating higher capacitance, supporting evidence that CoSe improves charge separation for water splitting.

The Mott Schottky plots (Figure 4.8a-b) provide further supporting evidence for CoSe as a facilitator of charge separation. The higher slope of (Figure 4.8a) FTO/Fe_2O_3 (5.27×10^{10}) compared to (Figure 4.8b) FTO/Fe_2O_3-CoSe (7.32×10^{9}) indicates a lower capacitance in the absence of CoSe catalyst. In addition to this, the Mott Schottky plots can be used to determine the charge carrier density N_D for each material (with an area A and relative permittivity ξ_r) using the following formula:[38]

$$N_D = \frac{1.41\times10^{32}(\mathrm{cm}\times\mathrm{F}^{-2}\times\mathrm{V}^{-1})}{\xi_r\times A^2(\mathrm{cm}^4)\times|slope|(\mathrm{F}^{-2}\times\mathrm{V}^{-1})} \quad (5.1)$$

Using the Mott Schottky slopes, a 1 cm^2 electrode area, and $\xi_r = 10$,[38] the N_D values were calculated to be 2.67×10^{20} in the absence of catalyst, and 1.93×10^{21} in the presence of catalyst. The increased charge carrier density in the presence of catalyst complements the previous observations that CoSe improves OER activity. The positive slope indicates n-type semi-conductivity, which is appropriate for OER.

4.4 Stability Study

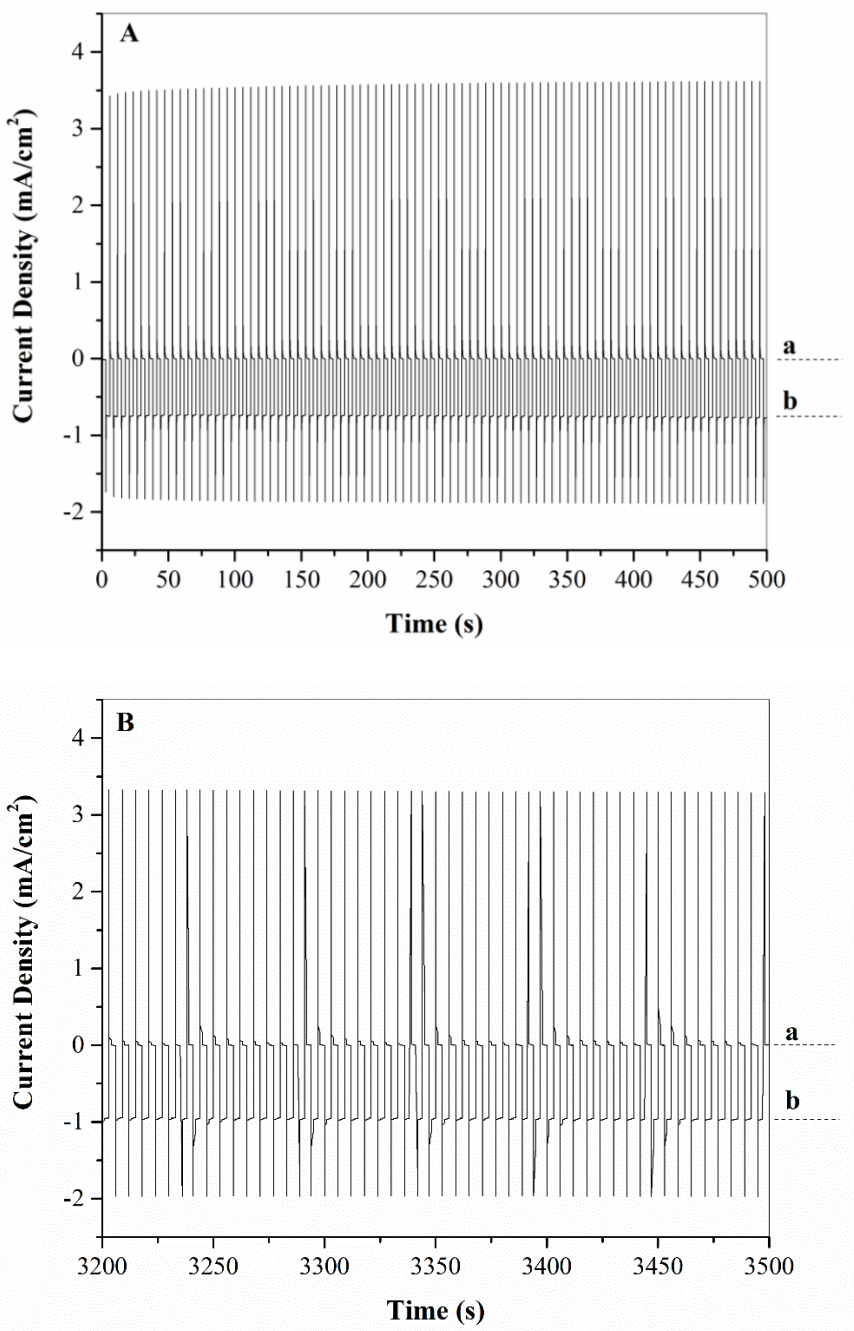

Figure 4.9 Stability study of FTO/Fe_2O_3 photoanodes under simulated solar radiation for the time region of (A) 0-500 s, and (B) 3200-3500 s. Potentials applied at (a) 0 V vs Ag/AgCl and (b) 1.10 V vs Ag/AgCl. The lack of significant change in current density indicates that the Fe_2O_3 film is very stable over time and does not decompose during OER.

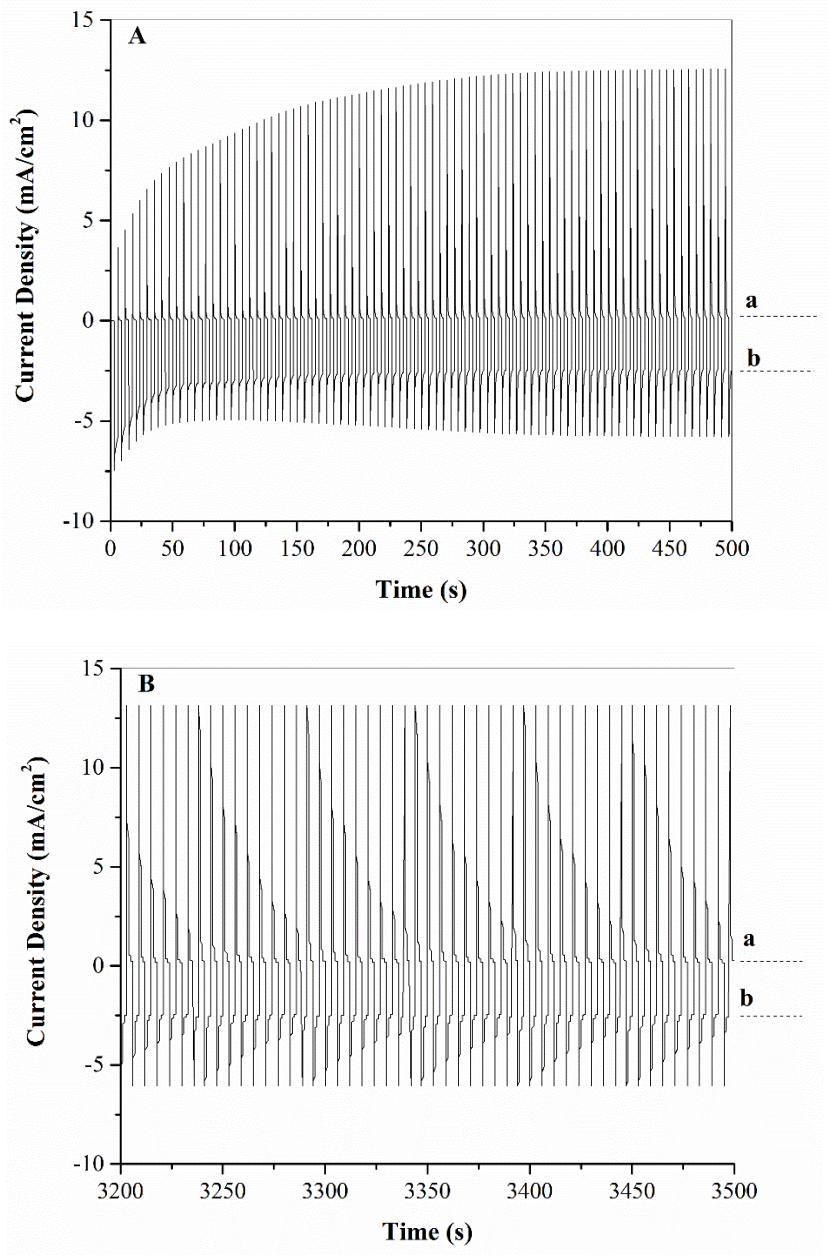

Figure 4.10 Stability study of FTO/Fe_2O_3-CoSe photoanodes under simulated solar radiation for the time region of (A) 0-500 s, and (B) 3200-3500 s. Potentials applied at (a) 0 V vs Ag/AgCl and (b) 1.10 V vs Ag/AgCl. An initial decrease in current density indicates some portion of the CoSe is not strongly bound to the electrode surface. For the remainder of time, little change is seen in current density, indicating the film remains stable after the initial loss of material.

The stabilities of FTO/Fe_2O_3 and FTO/Fe_2O_3-CoSe over time are shown in Figures 4.8 and 4.9, respectively. For FTO/Fe_2O_3, there is no significant decrease in current over time. The faradaic current remains stable near -0.97 mA/cm^2. For FTO/Fe_2O_3-CoSe, there is an initial significant decrease in current density from -6.98 mA/cm^2 to -3.80 mA/cm^2 within the first 50 seconds. After this period, it slowly decreases over time to 2.50 mA/cm^2. This suggests that the topmost layer of the CoSe is not strongly bound to the electrode, causing some of it to be removed during OER.

Chapter 5: Conclusion

FTO/Fe_2O_3-CoSe was studied as an earth-abundant photoanode for OER and compared to FTO/Fe_2O_3. The films were characterized using UV-vis spectroscopy, SEM, and EDX. The LSV measurements showed a significant increase in photocurrent in the presence of CoSe, indicating that CoSe acts as a catalyst for OER and increases electron/hole separation. This was confirmed by EIS and Mott Schottky plots, which showed increased capacitance and charge carrier density in the presence of CoSe. Future studies will focus on improving the stability of the CoSe catalyst to improve its current production over time by changing variables such as deposition bath composition, and pH. Different catalyst materials such as Mn_2O_3, NiSe, and WO_3 may be used with Fe_2O_3 and other photoanode materials such as $BiVO_4$ to probe other promising material combinations for photoelectrochemical water splitting.

Literature Cited

1. Grimes, C.A., Varghese, O.K., Ranjan, S.: Light, Water, Hydrogen – The Solar Generation of Hydrogen by Water Photoelectrolysis. Springer, New York (2008)
2. Song, F.; Hu, X. Exfoliation of layered double hydroxides for enhanced oxygen evolution catalysis, *Nature Communications*. **2014**, 5, 4477.
3. Meng, Y.; Song, W.; Huang, H.; Ren, Z.; Chen, S. Y.; Suib S. L. Structure-property relationship of bifunctional MnO2 nanostructures: highly efficient, ultra-stable electrochemical water oxidation and oxygen reduction reaction catalysts identified in alkaline media, *Journal of the American Chemical Society*. **2014**, 136, 11452-11464.
4. Gerken, J. B.; McAlpin, J. G.; Chen, J. Y.; Rigsby, M. L.; Casey, W. H.; Britt, R. D.; Stahl, S. S. Electrochemical water oxidation with cobalt-based electrocatalysts from pH 0-14: the thermodynamic basis for catalyst structure, stability, and activity, *Journal of the American Chemical Society*. **2011**, *133*, 14431.
5. Jiao, F.; Frei, H. Nanostructured cobalt and manganese oxide clusters as efficient water oxidation catalysts, *Energy and Environmental Science*. **2010**, 3, 1018-1027.
6. Matsumoto, Y.; Unal, U. Electrochemical approach to evaluate the mechanism of photocatalytic water splitting on oxide photocatalysts, *Journal of Solid State Chemistry*. **2004**, 177, 4205-4212.
7. Xia, C.; Jiang, Q.; Zhao, C.; Hedhili, M. N.; Alshareef, H. N. Selenide-based electrocatalysts and scaffolds for water oxidation applications, *Advanced Materials*. **2016**, 28, 77-85.

8. Lewis, N. S.; Nocera, D. G. Powering the Planet: chemical challenges in solar energy utilization, *Proceedings of the National Academy of Sciences of the United States of America*. **2006**, 103, 15729-15735.
9. van de Krol, R.; Grätzel, M. *Potoelectrochemical Hydrogen Production;* Electronic Materials: Science & Technology; Springer: New York, 2012; pp. 3-9.
10. Lewis, N.S., Crabtree, G.: *Basic Research Needs for Solar Energy Utilization: report of the Basic Energy Sciences Workshop on Solar Energy Utilization*, April 18-21, 2005. US Department of Energy, Office of Basic Energy Science, Washington, DC (2005).
11. Pacala, S.; Socolow, R. Stabilization Wedges: Solving the Climate Problem for the Next 50 Years with Current Technologies, *Science*. **2004**, 305, 968.
12. Hoffert, M. I. Farewell to Fossil Fuels? *Science*. **2010**, 329, 1292.
13. Krishnan Rajeshwar, R.M., Licht, S. *Solar Hydrogen Generation: Toward a Renewable Energy Future*; Springer: New York, 2008.
14. Grimes, C. A., Varghese, O.K., Ranjan, S. *Light, Water, Hydrogen*; Springer: New York, 2008.
15. Walter, M. G.; Warren, E. L.; McKone, J. R.; Boettcher, S. W.; Mi, Q.; Santori, E. A.; Lewis, N. S. Solar Water Splitting Cells *Chemical Reviews*. **2010**, 110, 6446.
16. Peter, L. M.; Wijayantha, K. G. U. Rate Law Analysis of Water Oxidation on a Hematite Surface, *J. Am. Chem. Soc.* **2015**, 15, 1983.
17. Qu, Y.; Duan, X. Progress, challenge and perspective of heterogeneous photocatalysts, *Chemical Society Reviews.* **2013**, 42, 2568.
18. Fujishima, A.; Honda, K. Electrochemical photolysis of water at a semiconductor electrode, *Nature*. **1972**, 238, 37.

19. Sivula, K.; Le Formal, F.; Grätzel, M. Solar Water Splitting: Progress Using Hematite (α-Fe2O3) Photoelectrodes, *Chem. Sus. Chem.* **2011**, 4, 432.
20. Sivula, K.; Gratzel, M. In *Photoelectrochemical Water Splitting: Materials, Processes and Architectures*; The Royal Society of Chemistry: 2013, pp. 83.
21. Ran, J.; Zhang, J.; Yu, J.; Jaroniec, M.; Qiao, S. Z. *Chemical Society Reviews* **2014**.
22. Yang, J.; Wang, D.; Han, H.; Li, C. Role of cocatalysts in photocatalysis and photoelectrocatalysis, *Accounts of Chemical Research* **2013**, 46, 1900.
23. Godwin, I. J.; Doyle, R. L.; Lyons, M. E. G. Water Oxidation Catalysis at RuO_2/NiO Mixed Oxide Electrodes, *Journal of the Electrochemical Society*. **2014**, 161, F906.
24. Stoerzinger, K. A.; Qiao, L.; Biegalski, M. D.; Shao-Horn, Y. Orientation-Dependent Oxygen Evolution Activities of Rutile IrO_2 and RuO_2, *Journal of Physical Chemistry Letters*. **2014**, 5, 1636.
25. Janaky, C.; Chanmanee, W.; Rajeshwar, K. On the Substantially Improved Photoelectrochemical Properties of Nanoporous WO_3 Through Surface Decoration with RuO_2, *Electrocatalysis*. **2013**, 4, 382.
26. Jeon, H. S.; Permana, A. D. C.; Kim, J.; Min, B. K. Water splitting for hydrogen production using a high surface area RuO_2 electrocatalyst synthesized in supercritical water *International Journal of Hydrogen Energy*. **2013**, 38, 6092.
27. Swierk, J. R.; McCool, N. S.; Saunders, T. P.; Barber, G. D.; Strayer, M. E.; Vargas-Barbosa, N. M.; Mallouk, T. E. Photovoltage effects of sintered IrO_2 nanoparticle catalysts in water-splitting dye-sensitized photoelectrochemical cells, *Journal of Physical Chemistry C*. **2014**, 118, 17046.

28. Hu, W.; Chen, S. L.; Xia, Q. H. IrO_2/Nb–TiO_2 electrocatalyst for oxygen evolution reaction in acidic medium, *International Journal of Hydrogen Energy*. **2014**, 39, 6967.
29. Xu, X.; Song, F.; Hu, X. A nickel iron diselenide-derived efficienct oxygen-evolution catalyst, *Nature Communications*. **2016**, 7, 12324.
30. Kwak, I. H.; Im, H. S.; Jang, D. M.; Kim, Y. W.; Park, K.; Lim, Y. R.; Cha, E. H.; Park, J. $CoSe_2$ and $NiSe_2$ Nanocrystals as Superior Bifunctional Catalysts for electrochemical and Photoelectrochemical Water Splitting, *ACS Applied Materials and Interfaces*. **2016**, 8, 5327.
31. Zhao, X.; Yang, Y.; Li, Y.; Cui, X.; Zhang, Y.; Xiao, P. NiCo-selenide as a novel catalyst for water oxidation, *Journal of Material Science*. **2016**, 51, 3724.
32. Xia, C.; Jiang, Q.; Zhao, C.; Hedhili, M N.; Alshareef, H. N. Selenide-Based Electrocatalysts and Scaffolds for Water Oxidation Applications, *Advanced Materials*. **2016**, 28, 77.
33. Anantharaj, S.; Ede, A. R.; Sakthikumar K.; Karthick, K.; Mishra, S.; Kundu, S. Recent Trends and Perspectives in Electrochemical Water Splitting with an Emphasis on Sulfide, Selenide, and Phosphide Catalysts of Fe, Co, and Ni: A Review, *ACS Catalysis*. **2016**, 6, 8069.
34. Schrebler, R.; Bello, K.; Vera, F.; Cury, P.; Muñoz, E.; del Río, R.; Meier H. G.; Córdova, R.; Dalchiele, E. A. An Electrochemical Deposition Route for Obtaining α-Fe_2O_3 Thin Films, *Electrochemical and Solid-State Letters*. **2006**, 9, 7, C110.
35. Lincot, D. *Thin Solid Films* **2005**, 487, 40.
36. Schwartz, R. W.; Schneller, T.; Waser, R. *Comptes Rendus Chimie* **2004**, 7, 433.

37. Liu, T.; Liu, Q.; Asiri, A. M.; Luo, Y.; Sun, X. An Amorphous CoSe Film Behaves as an Active and Stable Full Water-Splitting Electrocatalyst Under Strongly Alkaline Conditions, *Chemical Communications*. **2015**, 93, 16683.